Nonblinking, Intense Two-Dimensional Light Emitter: Monolayer WS_2 Triangles

Namphung Peimyoo,[†,‡] Jingzhi Shang,[†,‡] Chunxiao Cong,[†] Xiaonan Shen,[†] Xiangyang Wu,[§] Edwin K. L. Yeow,[†,§] and Ting Yu[†,⊥,∥,*]

[†]Division of Physics and Applied Physics, School of Physical and Mathematical Sciences, Nanyang Technological University, Singapore 637371, [§]Division of Chemistry and Biological Chemistry, School of Physical and Mathematical Sciences, Nanyang Technological University, Singapore 637371, [⊥]Department of Physics, Faculty of Science, National University of Singapore, Singapore 117542, and [∥]Graphene Research Centre, National University of Singapore, 2 Science Drive 3, Singapore 117542. [‡]N. Peimyoo and J. Shang contributed equally.

ABSTRACT Monolayer WS_2 (1L-WS_2), with a direct band gap, provides an ideal platform to investigate unique properties of two-dimensional semiconductors. In this work, light emission of a 1L-WS_2 triangle has been studied by using steady-state, time-resolved, and temperature-dependent photoluminescence (PL) spectroscopy. Two groups of 1L-WS_2 triangles have been grown by chemical vapor deposition, which exhibit nonuniform and uniform PL, respectively. Observed nonuniform PL features, *i.e.*, quenching and blue-shift in certain areas, are caused by structural imperfection and n-doping induced by charged defects. Uniform PL is found to be intrinsic, intense, and nonblinking, which are attributed to high crystalline quality. The binding energy of the A-exciton is extracted experimentally, which gives direct evidence for the large excitonic effect in 1L-WS_2. These superior photon emission features make 1L-WS_2 an appealing material for optoelectronic applications such as novel light-emitting and biosensing devices.

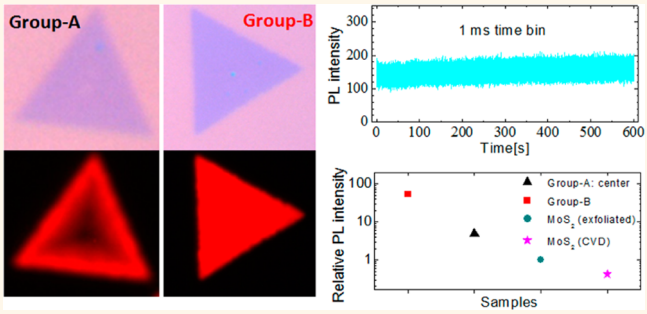

KEYWORDS: WS_2 · photoluminescence · CVD · microspectroscopy · temperature dependence

With the great research on graphene,[1−3] a series of two-dimensional (2D) materials have aroused considerable interest in the research community of fundamental sciences and device applications.[4−6] Recently, the direct-band-gap monolayers of several transition metal dichalcogenides (TMDs) such as 2H-MoS_2, 2H-$MoSe_2$, 2H-WS_2, and 2H-WSe_2 have shown attractive light emission properties in the visible and near-infrared spectral region.[7−12] Nowadays, widely used inorganic light-emitting devices are mainly based on direct-band-gap III−V semiconductors such as GaAs and GaN.[13−15] The newly emerging 2D direct-band-gap TMD semiconductors significantly enrich the present light-emitting applications.

Since 2010, the photoluminescence (PL) of monolayer MoS_2 (1L-MoS_2) has been studied in exfoliated,[7,16−18] chemically derived,[8] and chemical-vapor-deposition (CVD) grown samples.[19,20] The PL of MoS_2 could be substantially affected by the charge carrier concentration induced by substrates[20−22] or electrical gating,[23] and the surrounding environments (*e.g.*, solvatochromic effect) such as physically absorbed gas molecules[18] and solvents.[24] Due to the breaking of inversion symmetry and strong spin−orbital coupling, by using circular polarized light to stimulate the PL emission of 1L-MoS_2, the valley-selective circular dichroism and the control of the valley quantum number of electrons have been achieved,[25−27] which motivates the development of novel valleytronics.[28] Very recently, the PL from $MoSe_2$,[9,17,18] WS_2,[10,11,20,29] and WSe_2[9,10,18,29] has also been reported. Some groups have shown that 1L-WS_2 and 1L-WSe_2 on SiO_2/Si substrates have much stronger PL than that from 1L-MoS_2.[9,10]

Until now, although some progress has been made for the growing TMD monolayers, the PL investigation of 1L-WS_2 is still limited and controversial.[10,11,20,29] For example, a mechanically exfoliated 1L-WS_2 flake from synthetic bulk crystals has exhibited uniform PL;[10,29] in contrast, extraordinary PL has been observed near the edge of triangular 1L-WS_2 grown by CVD.[11] On the other hand, the CVD-grown 1L-WS_2 is expected to be more promising for extensive device applications than exfoliated 1L-WS_2

* Address correspondence to yuting@ntu.edu.sg.

Received for review September 3, 2013 and accepted November 22, 2013.

Published online November 22, 2013
10.1021/nn4046002

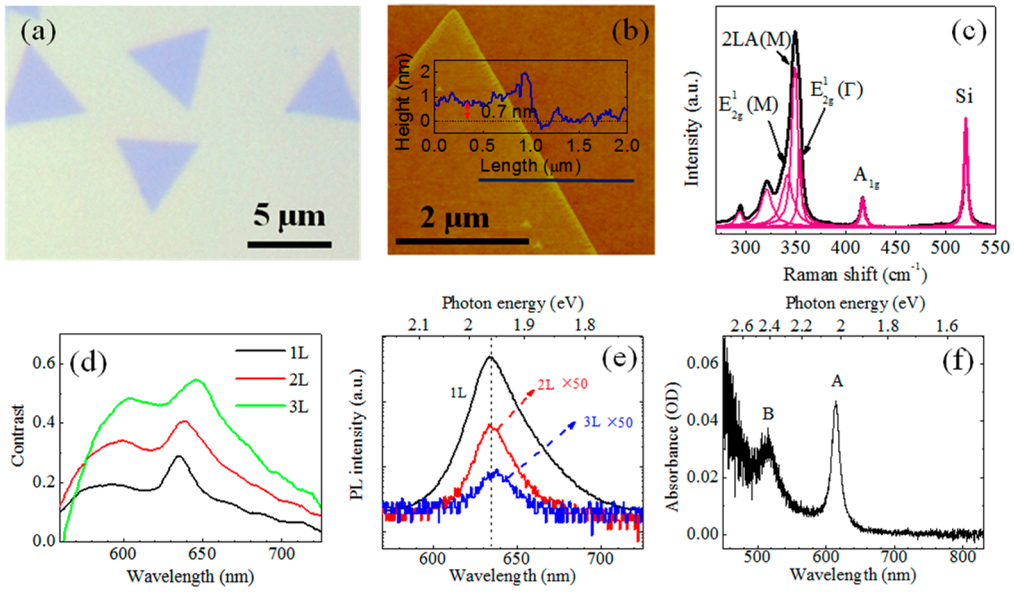

Figure 1. (a) Optical image of triangular 1L-WS_2 grown on a SiO_2/Si substrate. (b) AFM image of 1L-WS_2 and its corresponding height profile. (c) Multipeak Lorentzian fitting of Raman bands in 1L-WS_2. (d) Contrast spectra of WS_2 layers. (e) PL spectra from 1 to 3L WS_2 layers. (f) Absorption spectrum of 1L-WS_2 on quartz.

flakes in view of the technical controllability. Thus, we focus on the light emission studies of the CVD-grown 1L-WS_2 single crystal by micro-PL spectroscopy. Strong and uniform PL has been observed on high-quality 1L-WS_2 triangles. In the nonuniform samples, the darkening and the blue-shift of PL have been found to be related to as-grown structural defects. The thermal activation energy and the band gap of 1L-WS_2 have been estimated by low-temperature PL measurements. Time-resolved spectroscopic studies have shown the discrepant PL lifetimes among 1L-WS_2 samples prepared by different growth conditions.

RESULTS AND DISCUSSION

Figure 1a shows the optical image of individual 1L-WS_2 triangles as grown on a SiO_2/Si substrate. Figure 1b shows the atomic force microscopy (AFM) mapping of a triangle together with its height profile. The height of ~0.7 nm is indicative of 1L, in agreement with the previous studies.[10,11] In our samples, 1L-WS_2 triangles are predominant, and a minority of few-layer WS_2 flakes appear (Figure S1). Raman characteristics of 1L-WS_2 are shown in Figure 1c, which is obtained at the excitation wavelength (λ_{ex}) of 532 nm. The strongest peak at ~350 cm^{-1} comprises three subpeaks, which are resolved by multipeak Lorentzian fitting. According to the calculated phonon dispersion[30] and expermental studies[20,29,31,32] of 1L-WS_2, the peaks at 343, 350, and 355 cm^{-1} are assigned to the in-plane vibrational E^1_{2g} (M) mode, the second-order mode of longitudinal acoustic phonon 2LA (M), and the in-plane vibrational E^1_{2g} (Γ) mode, respectively; other peaks at 417, 296, and 320 cm^{-1} are attributed to the out-of-plane A_{1g} mode and the combination modes of 2LA-$2E^2_{2g}$ and 2LA-E^2_{2g}, respectively. The number of WS_2 layers can be estimated by Raman spectra as shown in Figure S2a and b, where the layer-number dependences of Raman band frequencies are presented.

Moreover, the number of thin layers is determined by contrast spectroscopy. Previous contrast measurements have shown the powerful ability to identify the numbers of graphene[33] and MoS_2 layers.[34] Figure 1d shows contrast spectra of 1−3L WS_2. For 1L-WS_2, the contrast spectrum has one peak around 635 nm, which is induced by the superposition of reflected, absorbed, and emitted photons from the WS_2/SiO_2/Si complex. The peak red-shifts with the increase in thickness, which is consistent with PL emission studies on the A-exciton discussed later. The contrast values at 600 nm were plotted as a function of thickness, showing the linear dispersion (Figure S2c).

Figure 1e shows the PL spectra of 1−3L WS_2 between 570 and 725 nm at λ_{ex} = 532 nm. The peak maxima appear in the spectral range of 630−640 nm. For 1L-WS_2, the peak mainly originates from A-exciton emission, *i.e.*, the direct excitonic transition between the lowest conduction band (CB) and the highest valence band (VB) at the same K point.[29] Note that the potential role of bound excitons and charged excitons in the observed emission band needs to be further investigated. The intensity dramatically increases when the thickness drops from 2L to 1L, indicating the transformation from indirect to direct band transitions. With the increase in thickness, the PL position red-shifts and the width broadens (Figure S3a). For the shift of PL position, the previous studies[10,11,29] show different results (Figure S3b and c). From 1L to 2L, a blue-shift of the A-exciton was observed by Gutierrez

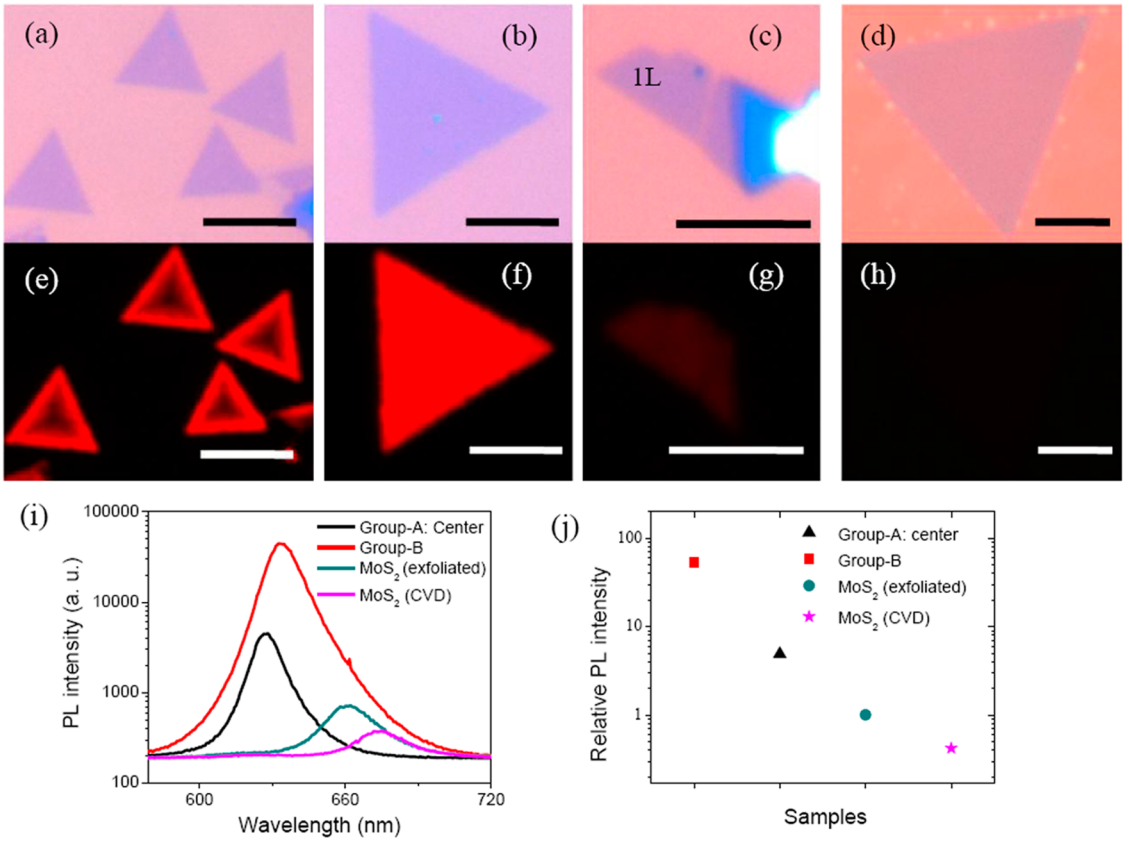

Figure 2. (a−d) Optical images of 1L-WS_2 triangles from group A, a 1L-WS_2 triangle from group B, exfoliated MoS_2 layers from natural crystals, and CVD-grown 1L-MoS_2, respectively. (e−h) Fluorescence images of 1L-WS_2 triangles (group A), a 1L-WS_2 triangle (group B), exfoliated MoS_2 layers, and CVD-grown 1L-MoS_2. (i) PL spectra from WS_2 and MoS_2 samples at λ_{ex} = 532 nm. (j) Comparison of integrated PL intensity of WS_2 and MoS_2 samples in which all values are normalized to the integrated PL intensity of exfoliated 1L-MoS_2. Scale bars represent 5 μm.

et al.,[11] while the red-shift was found by others.[10,29] Most probably, the discrepancy is due to the diverse electronic structures induced by different preparation processes. Previous studies on graphene layers have shown that misorientation of layer stacking occurs in exfoliated,[35,36] CVD-grown,[37] and epitaxial[38] graphene samples, which results in variable electronic transitions/stuctures. Figure 1f shows the absorption spectrum of a 1L-WS_2 sample on quartz. There are two absorption bands at 615 (2.02 eV) and 517 (2.40 eV) nm, corresponding to A and B excitonic transitions, with full widths at half-maximum of 47 and 133 meV, respectively. Furthermore, by use of a calibrated rhodamine 6G film (Figure S4), the PL quantum yield of 1L-WS_2 has been estimated referring to the previous approach[16] for 1L-MoS_2. The PL quantum yield of our 1L-WS_2 on quartz is ~2.0%, which is much larger than that (0.42%) of suspeneded 1L-MoS_2 exfoliated from the bulk MoS_2 crystal.[16] The relatively high PL quantum yield implies that 1L-WS_2 is a promising candidate for ultrathin 2D light-emitting applications.

Two groups of WS_2 samples have been grown under different heating conditions of the sulfur sources (described in the Materials and Methods section), named group A and group B, respectively. Figure 2a−h present optical and fluorescence images of 1L-WS_2 and 1L-MoS_2 samples on SiO_2/Si substrates. All fluorescence images and PL spectra were taken under identical conditions. The fluorescence image of 1L-WS_2 triangles of group A shows a nonuniform feature (Figure 2e); that is, the brightness gradually decreases from the outer to inner regions. In contrast to group A, the 1L-WS_2 triangle of group B presents a quite uniform brightness and the strongest intensity among all types of samples investigated in this work (Figure 2f). For the exfoliated MoS_2 sample (Figure 2g), the 1L region shows a uniform brightness, while the nearby bulk area cannot be seen due to the dominant emission band shifting to the infrared spectral region, which is out of the detection range of our system. The weak emission intensity from the CVD-grown 1L-MoS_2 is shown in Figure 2h (also see Figure S5 for the contrast-enhanced fluorescence image). Figure 2i presents the PL spectra from WS_2 and MoS_2 samples, where PL spectra were taken at λ_{ex} = 532 nm and the integrated intensities were collected in the spectral range 550−750 nm. Their relative integrated intensities are shown in Figure 2j, which are normalized to that from the exfoliated 1L-MoS_2. The integrated PL intensity of 1L-WS_2 (group B) is nearly 53 times that from the exfoliated 1L-MoS_2 at λ_{ex} = 532 nm. Note that the relative intensity ratio depends on λ_{ex}, caused by the

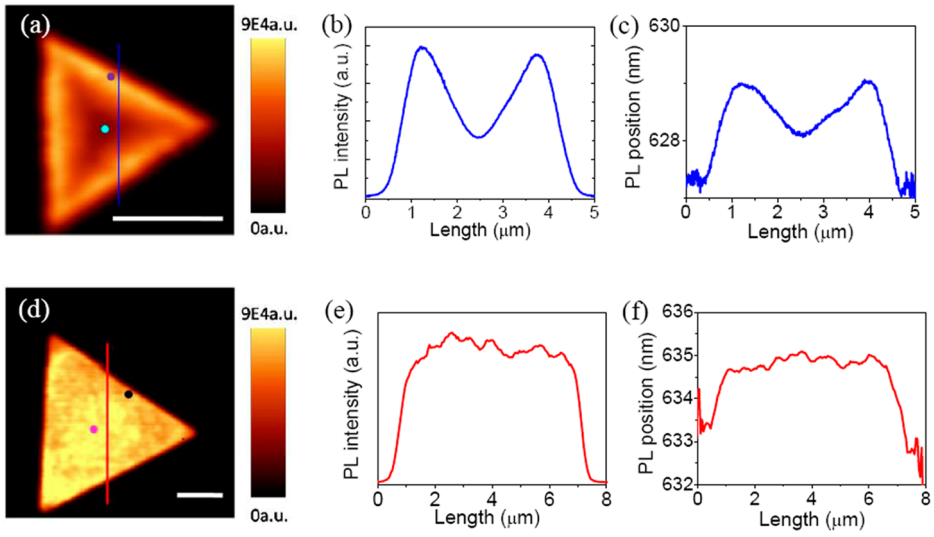

Figure 3. (a) PL mapping of an individual 1L-WS_2 triangle from group A. (b, c) Line scanning profiles of integrated PL intensity and PL peak position along the blue line in (a), respectively. (d) PL mapping of an individual 1L-WS_2 triangle from group B. (e, f) Line scanning profiles of the integrated PL intensity and the PL peak position along the red line in (d), respectively. Note that (a) and (d) were obtained under the same excitation conditions. Scale bars are 3 μm.

absorbance changes of 1L-WS_2 and 1L-MoS_2 at different excitation wavelengths (for example at λ_{ex} = 457 nm, the ratio becomes ~45 times; see details in Figure S6). For 1L-WS_2 exfoliated from the synthetic crystals, the previously reported PL intensity ratio of 1L-WS_2 to the exfoliated 1L-MoS_2 at λ_{ex} = 473 nm was between 20 and 30.[10]

To further understand the difference between two groups of samples, micro-PL spectroscopy is used to study the spatial PL distribution throughout the WS_2 triangles. Figure 3a shows the integrated PL intensity map of one triangle from group A, where the inner part shows a darker intensity than that of the outer. It is clarified by the PL spectra from the center (cyan dot) and outer (violet dot) regions (Figure S7a). Furthermore, line scanning profiles (Figure 3b and c) have shown the gradual evolution of the integrated intensity and peak position of PL along the blue line marked in Figure 3a. At the center region of the triangle, the PL intensity is darker than that of the edge and the PL peak exhibits a blue-shift with respect to the PL of the outer area. The PL spatial distribution is not random but exhibits the strongly correlated trait with the sample structure itself. Note that, for the different 1L-WS_2 flakes from group A, the PL widths vary from 40 to 60 meV and the PL maxima cover 1.96−1.98 eV. Similar nonuniform PL features of the 1L-WS_2 triangle have also been observed by others,[11] where the intensity, the width (42−68 meV), and the position (1.96−1.99 eV) of PL spatially fluctuate over the WS_2 triangles.

On the other hand, the relatively uniform PL from the WS_2 flakes was recently reported, while the spatial PL mapping from a single 1L-WS_2 triangle was missing.[20] Figure 3d shows an integrated PL intensity map of one 1L-WS_2 triangle from group B. The integrated intensity of PL is homogeneous and intense for the entire triangle, unlike group A samples, which is attributed to the high crystal quality. Meanwhile, PL spectra from the edge and the center regions (indicated by dots) are comparable (see Figure S7b). Figure 3e and f present the corresponding line scans of PL intensity and position, respectively, which further confirm the homogeneity of the sample. The widths and the positions of PL of the 1L-WS_2 triangles from group B are close to ~40 meV and ~1.96 eV, respectively. In addition, fluorescence images in Figure 2 correspond well to the PL intensity mappings (Figure 3), which suggests that the fluorescence microscopy is a rapid approach of analyzing the uniformity and the quality of thin WS_2 samples.

For the different observed intensities and positions of PL from two groups of samples, several factors may be responsible, including external electrostatic doping induced by the dielectric environment, strain, absorbates/clusters, and structural defects. Experimentally, Raman spectroscopy is a very powerful tool to estimate the electronic doping and strain in 2D materials, such as graphene,[39,40] MoS_2,[41,42] and WS_2.[11] In the typical 2H-type TMDs, the A_{1g} mode is sensitive to external electrostatic doping,[41] while the E^1_{2g} mode is responsive to the strain,[42] where the changes of positions and/or widths of Raman peaks are used to estimate the quantities of electrostatic doping and strain. The Raman mappings of A_{1g} and E^1_{2g} peak frequencies of two samples are shown in Figure S8. All Raman mappings exhibit spatial uniformity. In other words, both A_{1g} and E^1_{2g} Raman bands within the same triangle do not present relative changes of positions and/or widths induced by inhomogeneous external electrostatic doping and strain. Thus, neither external electrostatic doping from the dielectric environment or strain is

responsible for the PL nonuniformity. Experimentally, under the same surroundings and growth conditions, the structure-related gradient of PL (Figure 3a) is unlikely to be caused by the external electrostatic doping from the substrate or the atmosphere. To clarify the effect of absorbates/clusters on PL, AFM measurements have been carried out. Previous studies[43] have shown that the absorbates/clusters on graphene layers increase the surface roughness and/or the height. However, the obtained images (Figure S8a and d) have shown the high uniformity for our samples. Therefore, absorbates/clusters are ruled out for the observed differences of PL.

Conventionally, the defects in a semiconductor can lead to the quenching of intrinsic PL or act as nonradiative recombination sites.[19,44] The defect-induced electronic states within the band gap have been pointed out in early works.[45] Recently, high-resolution scanning transmission electron microscopic (STEM) measurements[19,46,47] have clearly shown various native and induced defects in 1L-MoS_2 as-grown by CVD, and the quenching PL at mirror grain boundaries containing line defects has been identified.[19] By modeling the defected atomic segments, the midgap states are present within the band gap of MoS_2.[19,46] In view of the very similar crystal structures and the same growth technique of 1L-WS_2 and 1L-MoS_2, analogous defects are highly expected to form in some WS_2 samples, in accordance with previous arguments.[46] Most probably, the defect-induced midgap states account for the observed PL quenching. Particularly, comparing the intensities of our group A with group B, the weaker PL in group A is attributed to the presence of localized electronic states induced by structural defects such as point defects and dislocations, which are formed during the growth procedure; within group A, the weakening of PL intensity of the inner region with respect to the outer region is attributed to more structural defects inside.

As shown in Figure 3c and f, we have observed the PL blue-shift of group A (or the inner part of group A) with respect to group B (or the outer part of group A). Similarly, the blue-shift of PL emission has been observed in regions of grain boundaries of the 1L-MoS_2 film,[19] which is explained by the possible doping and/or compressive strain induced by the boundary structures. In our single-crystal triangles of 1L-WS_2, there are no doping and strain caused by grain boundaries. Moreover, the blue-shift of the A-exciton has also been determined in gated 1L-MoS_2 devices, which is attributed to the modulated n-doping.[23] In our 1L-WS_2 triangle from group A, the surroundings of the inner and outer regions are quite similar; thus, only electrostatic doping due to the environment cannot result in the gradient evolution of the PL position. We further note that the influence of various defects on doping in MoS_2 has been discussed in theory[48,49] and experiment.[46,50−52] Cheng *et al.* have predicted the n-doping in 1L-MoS_2 caused by sulfur vacancies.[48] By use of angle-resolved photoemission spectroscopy, the dislocations in MoS_2 have been found to be negatively charged.[51] In n-doped MoS_2 nanoparticles, the blue-shift of the exciton energy was reported, where the rhenium atoms were used as substitutional dopants (*i.e.*, one kind of structural defect).[52] According to previous studies on native structural defects in MoS_2,[46,51] different amounts of charged defects, *i.e.*, vacancies of S (V_S), 2S (V_{2S}), and WS_3 (V_{WS3}) and dislocations, probably exist in the CVD-grown WS_2. Note that the structural defects have been observed in the CVD-grown atomically thin WS_2 film.[53] In our case, the PL blue-shift of group A with respect to group B is attributed to the localized n-doping induced by charged structural defects (*e.g.*, Vs) in WS_2. The blue-shift of PL within the samples from group A is interpreted in terms of the same charged-defect-induced n-doping, but with continuously varied doping concentrations from the center to the outer part. Note that the as-grown 1L-WS_2 by Lee *et al.* has shown n-doping in the electrical transport measurements of back-gated transistors,[20] which is consistent with our assignments above.

To further clarify the interpretation above, we have performed PL time-trace and electrical transport measurements. According to the previous studies,[54,55] continuous laser irradiation or plasma can induce atom sublimation accompanied by structural modification/defects and even thin the few-layer TMD materials. Thus, we performed PL time-trace measurements by use of a focused 532 nm laser beam with the power density of 1.4 kW/cm^2. With the increase in time (0−60 s), the decrease of PL intensity has been observed for group A samples, while both PL intensity and position remain stable for group B samples under the same conditions (Figure S9a−c). Moreover, for the exfoliated 1L-WS_2, it shows similar behaviors to those of group B (Figure S9d). These measurements have indicated group B and exfoliated 1L-WS_2 samples are more stable than group A samples under the same laser irradiation conditions. Furthermore, both weakening and blue-shift of PL in another group A sample were observed under a higher laser power density of 190 kW/cm^2 and an irradiation duration of 300 s, as shown in Figure S9e and f. With the probable atom sublimation/structural defects induced by laser beam, the observed PL intensity decrease and blue-shift are consistent with the defect-related explanation for group A and group B. The field effect transistor device by use of CVD-grown 1L-WS_2 (group B) has been fabricated, which shows a comparable electrical transport performance to that using exfoliated 1L-WS_2 (Figure S10). The results further demonstrate the compelling crystal quality of CVD-grown 1L-WS_2 for potential device applications.

Note that the inhomogeneous PL features have been observed in CVD-grown 1L-WS_2 triangles,[11] which are phenomenally similar to our observations of the sample from group A. In their studies,[11] the PL intensity near the edge was found to be 25 times higher than that at the center, which was attributed to the specific edge structure and chemical composition; the lower PL energy (red-shift) with respect to that in the center was explained by the inhomogeneity of the exciton binding energy. In our case, the relatively brighter PL emission at the edges of group A, and alternatively the darkening of PL near the center of the group A triangle, is assigned to the PL quenching by more structural defects inside the triangles. The blue-shift of the PL position near the center of the group A sample is assigned to the stronger defected-induced n-doping (negatively charged defects) than that near the edge. In a word, the PL emission is intense in more intrinsic regions of the 1L-WS_2 triangle. It is further confirmed by our observations of the 1L-WS_2 triangle from group B and the triangle-like exfoliated 1L-WS_2 (Figure S11), as well as other works[10,29] on the intense PL in the exfoliated 1L-WS_2.

Experimentally, the different PL properties of the two sample groups are correlated to the growth conditions as described in the Materials and Methods. In particular, for group A samples, the sulfur source was melted and evaporated by the furnace, where the temperature varied between room temperature and 300 °C during heating and cooling of the furnace; for group B samples, the sulfur source was loaded outside the furnace heat region and stably heated at 250 °C by an additional heater during the growth period (Figure S12). The nonuniform PL in group A is attributed to the relatively unstable supply of sulfur source resulting from the variation of the heating temperature and *vice versa* for group B. In our case, the commercial WO_3 powders were used as the tungsten precursor, which is different from the thermally evaporated ultrathin WO_3 films.[11] Compared with the previous seed-initiated growth,[20] no extra seed layer was used here, while an additional heater was introduced for the sulfur evaporation for group B samples. Note that the excess supply of sulfur, the cooling rate, the edge structures, and the substrate effect (the dielectric environment) may play roles in the TMD material growth and PL signals. For MoS_2 growth, oxisulfide rectangular flakes grew when the sulfur source was not adequate, while hexagonal and triangular MoS_2 were obtained with enough and excess sulfur supplies.[47] In our case, the excess sulfur was supplied during WS_2 growth. Previously, both natural[47] and fast cooling[19] have been used to grow high-quality MoS_2 samples. In particular, the large-size (>100 μm) MoS_2 triangle was prepared by CVD with a fast cooling rate.[19] In our case, natural cooling was used for the facile and repeatable operation of the CVD furnace. The edge geometries and chemical composition may affect the PL signals. For example, the second layer or thick layers of MoS_2 are prone to form at edge regions on the substrates,[47] which may result in the lower PL intensity near the sample edge. Recently, it was found that the PL signals of TMD materials varied on different substrates and fluctuated even on the same type of substrates.[22] Here, the same batch of SiO_2/Si wafers was chosen for two groups of 1L-WS_2 growth. Thus, the influence of the dielectric environment on the PL has been minimized among our samples.

Figure 4a and b show the temperature-dependent PL maps of 1L-WS_2 triangles of group A and group B, repsectively. The corresponding PL spectra are shown in Figure S13. In general, with the temperature rising from 80 to 380 K, the PL peak position presents a clear red-shift. Recently, in MoS_2[17,56] and $MoSe_2$[17] monolayers, similar PL shifts have also been observed. In Figure 4c, the integrated intensities of PL from both samples were plotted as functions of temperature. For group A, most intensities fluctuate between 2000 and 10000 counts. There is no apparent dependence found. In contrast, the PL intensity for group B presents a clear trend due to high uniformity and relatively low noise/signal ratio, which remains stable below 320 K and drops dramtically above 320 K. Previously, temperature-dependent PL measurements were used to determine the exciton binding energies in bulk[57,58] and some quasi-2D materials.[59] Recently, the PL intensity changes with temperature have also been correlated to the thermal dissociation of charged excitons in monolayer 2D $MoSe_2$ samples.[12] Here, we mainly consider the observed PL intensity changes due to thermal dissociation of excitons. The temperature-dependent PL integrated intensities of group B have been further fitted by a modified Arrhenius law,[60,61] and the fitting parameters are listed in Table S1. A single thermal activation energy of ~0.53 eV is extracted for group B, which could result from deep donor and/or acceptor trap states or the intrinsic binding energy of the A-exciton. In our case, the energy is extracted from the group B sample with higher quality rather than that of group A; this value is consistent with the recently calculated binding energy (about 0.5 eV) of the A-exciton in WS_2 by theoretical groups.[62,63] Thus, it is assigned to the intrinsic binding energy of the A-exciton rather than deep trap states, which gives strong experimental evidence for the existence of the predicted large excitonic effect in 1L-WS_2.[62−66] Note that other factors could also contribute to the temperarure-dependent changes of PL intensity. Another typical factor for decreased PL intensity is due to the rising probability of nonradiative recombination processes, which competes with radiative transitions with increasing temperature. In addition, the potential doping, strain, structural defects, the dielectric environment,[22] intrinsic band structure,[17]

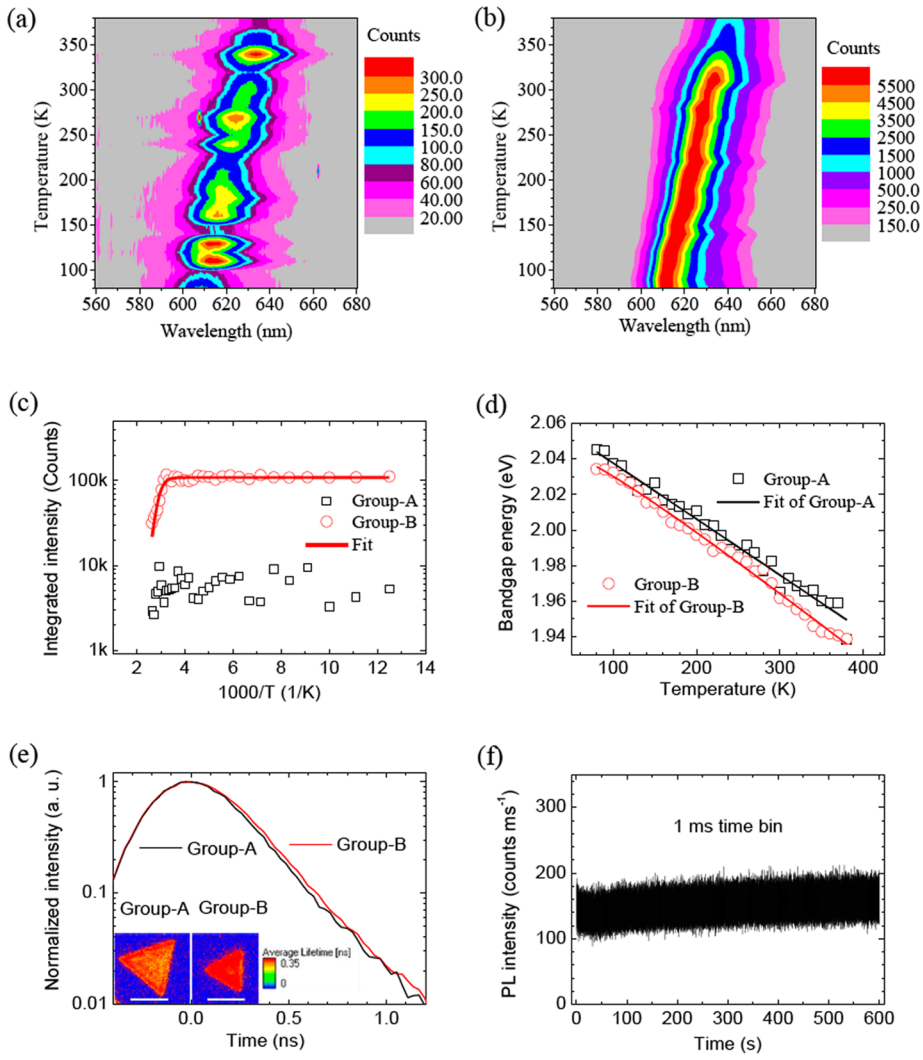

Figure 4. (a, b) Temperature-dependent PL maps of 1L-WS_2 triangles from groups A and B, respectively. (c) Integrated PL intensity as a function of temperature ranging between 80 and 380 K of two groups of samples. (d) Temperature dependences of PL peak positions of group A (opened square) and group B (opened circle), respectively. (e) Fluorescence kinetics and the lifetime images (inset) of two groups of samples. Scale bars represent 10 μm. (f) PL intensity as a function of the excitation time.

and many-body effects in low-dimensional structures may also affect the temperature-dependence behaviors of PL. For instance, the emission of defect-related bound excitons or environment-related surface states could cause the low-energy tail in the asymmetric PL band (Figure S14), and such emitting states may chanllenge A excitonic emission at low temperature. Similarly, the low-energy bands and/or competition among emission states have also been observed in the exfoliated 1L-MoS_2 at various temperatures[22,56,67] and in the 1L-$MoSe_2$ device sample.[12]

Meanwhile, the temperature-dependent PL positions (Figure 4d) are fitted by the empirical Varshni function,[68] *i.e.*, $E_g(T) = E_0 - \alpha T^2/(T + \beta)$. The fitting parameters α for groups A and B are 3.1×10^{-4} and 3.7×10^{-4} eV/K, respectively. The other parameters β for both samples are ~0 and 90 K, respectively. The band-gap energies at $T = 0$ K for both samples are ~2.07 and ~2.05 eV, respectively. The obtained larger band gap in group A than group B is consistent with the previous PL measurements (Figure 3). Futhermore, to estimate the electron−phonon interaction in 1L-WS_2, we have carried out another fitting (Figure S15) for the group B sample by use of a semiempirical function developed by Odonnell *et al.*,[69]

$$E_g(T) = E_0 - S\langle\hbar\omega_p\rangle[\coth(\langle\hbar\omega_p\rangle/2kT) - 1] \quad (1)$$

The obtained S is ~2.1, which characterizes the electron−phonon coupling stength and is slightly larger than those recently obtained from 1L-MoS_2 and 1L-$MoSe_2$.[12,17] The average phonon energy $\langle\hbar\omega_p\rangle$ is determined as ~14.5 meV (117 cm^{-1}) in 1L-WS_2. The PL width dependence of the group B sample on temperature is shown in Figure S16. When T < 300 K, the PL width is relatively stable, *i.e.*, ~40 meV; when T > 300 K, the broadening of the PL width is observed.

Figure 4e presents time-resolved PL kinetics collected from the centers of two groups of samples. Each decay curve presents an instrument-response-limited decay time (<350 ps). The corresponding lifetime images are also presented as the inset. Both data confirm that group B shows a relatively longer lifetime than group A. For group A, the inner region with the weaker PL intensity shows a shorter lifetime than the outer region. Figure 4f shows the time trace of the PL intensity of 1L-WS_2 from group B. Over a long duration of 600 s, the intensity remains stable/nonblinking. Conventionally, the blinking traits of light emission have been observed from most 0D and 1D semiconductor nanocrystals, including quantum dots, nanorods, nanowires, and nanotubes,[70−72] which cause the unpredicted emission intensity and severely limit biological and optical applications of nanocrystals. Here, 1L-WS_2 trangle, as a rising 2D semiconductor nanocrystal, shows a nonblinking PL feature, which opens up a great deal of opportunities for ultilization in optoeletronics, quantum optics, and biology, such as light-emitting, biosensing, and biolabeling materials. Particularly, the actual 2D semiconductor nanocrystals, owning intense and nonblinking light emission features, are good candidates to be used as active media in vertical cavity surface emission lasers, instead of conventional quasi-2D quantum wells.

CONCLUSIONS

To summarize, the PL of 1L-WS_2 triangle has been studied by use of micro-PL spectroscopy. Two groups of samples with uniform and nonuniform PL were compared to identify the native emission traits of 1L-WS_2. The darkening and the blue-shift of PL are explained by the as-grown structural defects and the defect-induced negative doping. In addition to the PL and Raman techniques, the optical contrast has successfully been used to identify the number of WS_2 layers. Moreover, the binding energy (0.53 eV) of the A-exciton has been determined by temperature-dependent measurements of PL, which evidence the large excitonic effect in 2D 1L-WS_2. More importantly, the intrinsic PL of 1L-WS_2 is found to be intense, *i.e.*, 53 times that of exfoliated 1L-MoS_2 at 532 nm excitation, and nonblinking, *i.e.*, stable during 10 min of continuous laser irradiation. These features make the novel 2D WS_2 semiconductor very attractive in advanced light-emitting and biosensing applications.

MATERIALS AND METHODS

Two groups of 1L-WS_2 samples were grown by chemical vapor deposition in a tube furnace referring to previous works on MoS_2.[19,47] Commercial WO_3 (>99.5%, Sigma Aldrich) and sulfur (>99.95%, Sigma Aldrich) were used as solid sources. For group A samples, 1 mg of WO_3 powder was put into the tube center and 200 mg of sulfur was loaded near the inlet of high-purity Ar carrier gas. The flow rate was 200 sccm during the whole growth procedure. The temperature was raised to 550 °C with a ramping rate of 18 °C/min. At this temperature, the sulfur started to melt due to the heating from the furnace itself, being similar to previous studies.[47] After that, the ramping rate was set at 5 °C/min. Later on, the temperature approached 800 °C and was held for 10 min. Then the furnace was cooled to room temperature naturally with the flow of Ar gas. For group B samples, 200 mg of sulfur was loaded upstream and outside of the furnace heating zone, which was heated separately at 250 °C. All other growth parameters are the same as those used for group A samples. By use of a modified transfer strategy,[19] two samples from group A and group B, respectively, were displaced onto the quartz substrates for absorption and time-resolved photoluminescence measurements. The exfoliated 1L-WS_2 samples on the SiO_2/Si substrate were obtained by micromechanical cleavage[1] of the bulk-synthesized WS_2 crystal (2D Semiconductors Inc.). Optical and fluorescence images were taken under an Olympus microscope (BX51) with a fluorescence attachment (U-RFL-T). A Raman/PL microscope setup (WITec, CRM 200) with a 532 nm diode-pumped double-frequency Nd:YAG laser source was employed for detecting both Raman and PL spectra. A thermal stage with a vacuum pump and the N_2 carrier gas was used in temperature-dependent PL measurements. An atomic force microscope (AFM, Veeco, Nanoscope V) was utilized to obtain the morphology images and the height profiles. Steady-state absorption and fluorescence spectra of the R6G solution and films were measured by use of a UV−vis absorption spectrometer (Cary 100, Varian) and a fluorescence spectrometer (Eclipse, Varian), respectively. The FTIR microspectrometer (Bruker Vertex 80v) was used to determine the absorption spectrum of 1L-WS_2 on quartz. Fluorescence lifetime imaging of WS_2 was obtained by use of a time-resolved confocal microscope (PicoQuant, MicroTime 200). A 405 nm pulsed laser (PicoQuant, LDH-P-C-405B) with a repetition rate of ~40 MHz and a power of ~0.15 μW was used to excite the samples, and the fluorescence ranging from 610 to 700 nm was detected by a single-photon avalanche diode (Perkin-Elmer, SPCM-AQR-15).

Conflict of Interest: The authors declare no competing financial interest.

Supporting Information Available: Optical and AFM images of as-grown WS_2 samples; Raman spectra of mono-, bi-, and trilayer and bulk WS_2; comparison of PL positions and widths as a function of the number of layers from previous reports and the present work; optical spectra of the R6G solution and the R6G film; relative intensities of 1L-WS_2 and 1L-MoS_2 samples at λ_{ex} = 457 nm; PL spectra from the edge and center regions of 1L-WS_2 triangles from two groups; AFM and Raman mapping images of 1L-WS_2 from two groups; PL time-trace data; electrical transport characteristics; optical images and PL spectrum from exfoliated 1L-WS_2; schematics of CVD setups; temperature-dependent PL spectra; temperature dependence of PL widths of 1L-WS_2 from group B; fit of PL spectra and the fitting parameters. This material is available free of charge *via* the Internet at http://pubs.acs.org.

Acknowledgment. We thank Prof. Cesare Soci and Mr. Zilong Wang for their help with the absorption measurements. This work is supported by the Singapore National Research Foundation under NRF Award No. NRF-RF2010-07 and MOE Tier 2 MOE2012-T2-2-049.

REFERENCES AND NOTES

1. Geim, A. K.; Novoselov, K. S. The Rise of Graphene. *Nat. Mater.* **2007**, *6*, 183–191.
2. Geim, A. K. Graphene: Status and Prospects. *Science* **2009**, *324*, 1530–1534.
3. Novoselov, K. S. Graphene: Materials in the Flatland. *Rev. Mod. Phys.* **2011**, *83*, 837–849.

4. Neto, A. H. C.; Novoselov, K. New Directions in Science and Technology: Two-Dimensional Crystals. *Rep. Prog. Phys.* **2011**, *74*, 82501–82509.
5. Xu, M.; Liang, T.; Shi, M.; Chen, H. Graphene-Like Two-Dimensional Materials. *Chem. Rev.* **2013**, *113*, 3766–3798.
6. Osada, M.; Sasaki, T. Two-Dimensional Dielectric Nanosheets: Novel Nanoelectronics from Nanocrystal Building Blocks. *Adv. Mater.* **2012**, *24*, 210–228.
7. Splendiani, A.; Sun, L.; Zhang, Y. B.; Li, T. S.; Kim, J.; Chim, C. Y.; Galli, G.; Wang, F. Emerging Photoluminescence in Monolayer MoS_2. *Nano Lett.* **2010**, *10*, 1271–1275.
8. Eda, G.; Yamaguchi, H.; Voiry, D.; Fujita, T.; Chen, M. W.; Chhowalla, M. Photoluminescence from Chemically Exfoliated MoS_2. *Nano Lett.* **2011**, *11*, 5111–5116.
9. Tonndorf, P.; Schmidt, R.; Bottger, P.; Zhang, X.; Borner, J.; Liebig, A.; Albrecht, M.; Kloc, C.; Gordan, O.; Zahn, D. R. T. *et al*. Photoluminescence Emission and Raman Response of Monolayer MoS_2, $MoSe_2$, and WSe_2. *Opt. Express* **2013**, *21*, 4908–4916.
10. Zhao, W. J.; Ghorannevis, Z.; Chu, L. Q.; Toh, M. L.; Kloc, C.; Tan, P. H.; Eda, G. Evolution of Electronic Structure in Atomically Thin Sheets of WS_2 and WSe_2. *ACS Nano* **2013**, *7*, 791–797.
11. Gutierrez, H. R.; Perea-Lopez, N.; Elias, A. L.; Berkdemir, A.; Wang, B.; Lv, R.; Lopez-Urias, F.; Crespi, V. H.; Terrones, H.; Terrones, M. Extraordinary Room-Temperature Photoluminescence in WS_2 Triangular Monolayers. *Nano Lett.* **2012**, *13*, 3447–3454.
12. Ross, J. S.; Wu, S.; Yu, H.; Ghimire, N. J.; Jones, A. M.; Aivazian, G.; Yan, J.; Mandrus, D. G.; Xiao, D.; Yao, W.; *et al*. Electrical Control of Neutral and Charged Excitons in a Monolayer Semiconductor. *Nat. Commun.* **2013**, *4*, 1474.
13. Pimputkar, S.; Speck, J. S.; DenBaars, S. P.; Nakamura, S. Prospects for LED Lighting. *Nat. Photonics* **2009**, *3*, 180–182.
14. Ponce, F. A.; Bour, D. P. Nitride-Based Semiconductors for Blue and Green Light-Emitting Devices. *Nature* **1997**, *386*, 351–359.
15. Brandt, O.; Ploog, K. H. Solid-State Lighting: The Benefit of Disorder. *Nat. Mater.* **2006**, *5*, 769–770.
16. Mak, K. F.; Lee, C.; Hone, J.; Shan, J.; Heinz, T. F. Atomically Thin MoS2: A New Direct-Gap Semiconductor. *Phys. Rev. Lett.* **2010**, *105*, 136805.
17. Tongay, S.; Zhou, J.; Ataca, C.; Lo, K.; Matthews, T. S.; Li, J. B.; Grossman, J. C.; Wu, J. Q. Thermally Driven Crossover from Indirect toward Direct Bandgap in 2D Semiconductors: $MoSe_2$ *versus* MoS_2. *Nano Lett.* **2012**, *12*, 5576–5580.
18. Tongay, S.; Zhou, J.; Ataca, C.; Liu, J.; Kang, J. S.; Matthews, T. S.; You, L.; Li, J.; Grossman, J. C.; Wu, J. Broad-Range Modulation of Light Emission in Two-Dimensional Semiconductors by Molecular Physisorption Gating. *Nano Lett.* **2013**, *13*, 2831–2836.
19. van der Zande, A. M.; Huang, P. Y.; Chenet, D. A.; Berkelbach, T. C.; You, Y.; Lee, G. H.; Heinz, T. F.; Reichman, D. R.; Muller, D. A.; Hone, J. C. Grains and Grain Boundaries in Highly Crystalline Monolayer Molybdenum Disulphide. *Nat. Mater.* **2013**, *12*, 554–561.
20. Lee, Y. H.; Yu, L. L.; Wang, H.; Fang, W. J.; Ling, X.; Shi, Y. M.; Lin, C. T.; Huang, J. K.; Chang, M. T.; Chang, C. S.; *et al*. Synthesis and Transfer of Single-Layer Transition Metal Disulfides on Diverse Surfaces. *Nano Lett.* **2013**, *13*, 1852–1857.
21. Yan, R.; Bertolazzi, S.; Brivio, J.; Fang, T.; Konar, A.; Birdwell, A. G.; Nguyen, N. V.; Kis, A.; Jena, D.; Xing, H. G. Raman and Photoluminescence Study of Dielectric and Thermal Effects on Atomically Thin MoS_2. 2012, arXiv: materials science/1211.4136v1. arXiv.org e-Print arXiv. http://arxiv.org/abs/1211.4136v1 (accessed Aug 17, 2013).
22. Sercombe, D.; Schwarz, S.; Del Pozo-Zamudio, O.; Liu, F.; Robinson, B. J.; Chekhovich, E. A.; Tartakovskii, I. I.; Kolosov, O.; Tartakovskii, A. I. Optical Investigation of the Natural Electron Doping in Thin MoS_2 Films Deposited on Dielectric Substrates. 2013, arXiv: materials science/1304.7221v3. arXiv.org e-Print arXiv. http://arxiv.org/abs/1304.7221v3 (accessed Aug 17, 2013).
23. Mak, K. F.; He, K. L.; Lee, C.; Lee, G. H.; Hone, J.; Heinz, T. F.; Shan, J. Tightly Bound Trions in Monolayer MoS_2. *Nat. Mater.* **2013**, *12*, 207–211.
24. Mao, N. N.; Chen, Y. F.; Liu, D. M.; Zhang, J.; Xie, L. M. Solvatochromic Effect on the Photoluminescence of MoS_2 Monolayers. *Small* **2013**, *9*, 1312–1315.
25. Mak, K. F.; He, K. L.; Shan, J.; Heinz, T. F. Control of Valley Polarization in Monolayer MoS_2 by Optical Helicity. *Nat. Nanotechnol.* **2012**, *7*, 494–498.
26. Zeng, H. L.; Dai, J. F.; Yao, W.; Xiao, D.; Cui, X. D. Valley Polarization in MoS_2 Monolayers by Optical Pumping. *Nat. Nanotechnol.* **2012**, *7*, 490–493.
27. Cao, T.; Wang, G.; Han, W. P.; Ye, H. Q.; Zhu, C. R.; Shi, J. R.; Niu, Q.; Tan, P. H.; Wang, E.; Liu, B. L.; *et al*. Valley-Selective Circular Dichroism of Monolayer Molybdenum Disulphide. *Nat. Commun.* **2012**, *3*, 887.
28. Behnia, K. Polarized Light Boosts Valleytronics. *Nat. Nanotechnol.* **2012**, *7*, 488–489.
29. Zeng, H. L.; Liu, G. B.; Dai, J. F.; Yan, Y. J.; Zhu, B. R.; He, R. C.; Xie, L.; Xu, S. J.; Chen, X. H.; Yao, W.; *et al*. Optical Signature of Symmetry Variations and Spin-Valley Coupling in Atomically Thin Tungsten Dichalcogenides. *Sci. Rep.* **2013**, *3*, 1608.
30. Molina-Sanchez, A.; Wirtz, L. Phonons in Single-Layer and Few-Layer MoS_2 and WS_2. *Phys. Rev. B* **2011**, *84*, 155413.
31. Berkdemir, A.; Gutierrez, H. R.; Botello-Mendez, A. R.; Perea-Lopez, N.; Elias, A. L.; Chia, C. I.; Wang, B.; Crespi, V. H.; Lopez-Urias, F.; Charlier, J. C.; *et al*. Identification of Individual and Few Layers of WS_2 Using Raman Spectroscopy. *Sci. Rep.* **2013**, *3*, 1755.
32. Zhao, W.; Ghorannevis, Z.; Kumar, A. K.; Pang, J. R.; Toh, M.; Zhang, X.; Kloc, C.; Tan, P. H.; Eda, G. Lattice Dynamics in Mono- and Few-Layer Sheets of WS_2 and WSe_2. *Nanoscale* **2013**, *5*, 9677–9683.
33. Ni, Z. H.; Wang, H. M.; Kasim, J.; Fan, H. M.; Yu, T.; Wu, Y. H.; Feng, Y. P.; Shen, Z. X. Graphene Thickness Determination Using Reflection and Contrast Spectroscopy. *Nano Lett.* **2007**, *7*, 2758–2763.
34. Castellanos-Gomez, A.; Agrait, N.; Rubio-Bollinger, G. Optical Identification of Atomically Thin Dichalcogenide Crystals. *Appl. Phys. Lett.* **2010**, *96*, 213116.
35. Cong, C. X.; Yu, T.; Sato, K.; Shang, J. Z.; Saito, R.; Dresselhaus, G. F.; Dresselhaus, M. S. Raman Characterization of ABA- and ABC-Stacked Trilayer Graphene. *ACS Nano* **2011**, *5*, 8760–8768.
36. Lui, C. H.; Li, Z. Q.; Chen, Z. Y.; Klimov, P. V.; Brus, L. E.; Heinz, T. F. Imaging Stacking Order in Few-Layer Graphene. *Nano Lett.* **2011**, *11*, 164–169.
37. Reina, A.; Jia, X. T.; Ho, J.; Nezich, D.; Son, H. B.; Bulovic, V.; Dresselhaus, M. S.; Kong, J. Large Area, Few-Layer Graphene Films on Arbitrary Substrates by Chemical Vapor Deposition. *Nano Lett.* **2009**, *9*, 30–35.
38. Hass, J.; Varchon, F.; Millan-Otoya, J. E.; Sprinkle, M.; Sharma, N.; De Heer, W. A.; Berger, C.; First, P. N.; Magaud, L.; Conrad, E. H. Why Multilayer Graphene on 4H-SiC($000\bar{1}$) Behaves Like a Single Sheet of Graphene. *Phys. Rev. Lett.* **2008**, *100*, 125504.
39. Das, A.; Pisana, S.; Chakraborty, B.; Piscanec, S.; Saha, S. K.; Waghmare, U. V.; Novoselov, K. S.; Krishnamurthy, H. R.; Geim, A. K.; Ferrari, A. C.; *et al*. Monitoring Dopants by Raman Scattering in an Electrochemically Top-Gated Graphene Transistor. *Nat. Nanotechnol.* **2008**, *3*, 210–215.
40. Huang, M. Y.; Yan, H. G.; Chen, C. Y.; Song, D. H.; Heinz, T. F.; Hone, J. Phonon Softening and Crystallographic Orientation of Strained Graphene Studied by Raman Spectroscopy. *Proc. Nat. Acad. Sci.* **2009**, *106*, 7304–7308.
41. Chakraborty, B.; Bera, A.; Muthu, D. V. S.; Bhowmick, S.; Waghmare, U. V.; Sood, A. K. Symmetry-Dependent Phonon Renormalization in Monolayer MoS_2 Transistor. *Phys. Rev. B* **2012**, *85*, 161403(R).
42. Wang, Y.; Cong, C. X.; Qiu, C.; Yu, T. Raman Spectroscopy Study of Lattice Vibration and Crystallographic Orientation of Monolayer MoS_2 under Uniaxial Strain. *Small* **2013**, DOI: 10.1002/smll.201202876.
43. Peimyoo, N.; Yu, T.; Shang, J. Z.; Cong, C. X.; Yang, H. P. Thickness-Dependent Azobenzene Doping in Mono- and Few-Layer Graphene. *Carbon* **2012**, *50*, 201–208.

44. Pankove, J. I. *Optical Processes in Semiconductors*; Prentice Hall: NJ, 1971.
45. Pantelides, S. T. The Electronic Structure of Impurities and Other Point Defects in Semiconductors. *Rev. Mod. Phys.* **1978**, *50*, 797–858.
46. Zhou, W.; Zou, X.; Najmaei, S.; Liu, Z.; Shi, Y.; Kong, J.; Lou, J.; Ajayan, P. M.; Yakobson, B. I.; Idrobo, J. C. Intrinsic Structural Defects in Monolayer Molybdenum Disulfide. *Nano Lett.* **2013**, *13*, 2615–2622.
47. Najmaei, S.; Liu, Z.; Zhou, W.; Zou, X.; Shi, G.; Lei, S.; Yakobson, B. I.; Idrobo, J.-C.; Ajayan, P. M.; Lou, J. Vapor Phase Growth and Grain Boundary Structure of Molybdenum Disulfide Atomic Layers. *Nat. Mater.* **2013**, *12*, 754–759.
48. Cheng, Y. C.; Zhu, Z. Y.; Mi, W. B.; Guo, Z. B.; Schwingenschlogl, U. Prediction of Two-Dimensional Diluted Magnetic Semiconductors: Doped Monolayer MoS_2 Systems. *Phys. Rev. B* **2013**, *87*, 100401(R).
49. Enyashin, A. N.; Bar-Sadan, M.; Houben, L.; Seifert, G. Line Defects in Molybdenum Disulfide Layers. *J. Phys. Chem. C* **2013**, *117*, 10842–110848.
50. Komsa, H. P.; Kotakoski, J.; Kurasch, S.; Lehtinen, O.; Kaiser, U.; Krasheninnikov, A. V. Two-Dimensional Transition Metal Dichalcogenides under Electron Irradiation: Defect Production and Doping. *Phys. Rev. Lett.* **2012**, *109*, 035503.
51. Mahatha, S. K.; Menon, K. S. R. Inhomogeneous Band Bending on MoS_2(0001) Arising from Surface Steps and Dislocations. *J. Phys.: Condens. Matter* **2012**, *24*, 305502.
52. Sun, Q. C.; Yadgarov, L.; Rosentsveig, R.; Seifert, G.; Tenne, R.; Musfeldt, J. L. Observation of a Burstein-Moss Shift in Rhenium-Doped MoS_2 Nanoparticles. *ACS Nano* **2013**, *7*, 3506–3511.
53. Elías, A. L.; Perea-López, N.; Castro-Beltrán, A.; Berkdemir, A.; Lv, R.; Feng, S.; Long, A. D.; Hayashi, T.; Kim, Y. A.; Endo, M. Controlled Synthesis and Transfer of Large Area WS_2 Sheets: From Single-Layer to Few-Layers. *ACS Nano* **2013**, *7*, 5235–5242.
54. Castellanos-Gomez, A.; Barkelid, M.; Goossens, A. M.; Calado, V. E.; van der Zant, H. S. J.; Steele, G. A. Laser-Thinning of MoS_2: On Demand Generation of a Single-Layer Semiconductor. *Nano Lett.* **2012**, *12*, 3187–3192.
55. Liu, Y.; Nan, H.; Wu, X.; Pan, W.; Wang, W.; Bai, J.; Zhao, W.; Sun, L.; Wang, X.; Ni, Z. Layer-by-Layer Thinning of MoS_2 by Plasma. *ACS Nano* **2013**, *7*, 4202–4209.
56. Korn, T.; Heydrich, S.; Hirmer, M.; Schmutzler, J.; Schuller, C. Low-Temperature Photocarrier Dynamics in Monolayer MoS_2. *Appl. Phys. Lett.* **2011**, *99*, 102109.
57. Hal Bogardus, E.; Barry Bebb, H. Bound-Exciton, Free-Exciton, Band-Acceptor, Donor-Acceptor, and Auger Recombination in GaAs. *Phys. Rev.* **1968**, *176*, 993–1002.
58. Reshchikov, M. A.; Korotkov, R. Y. Analysis of the Temperature and Excitation Intensity Dependencies of Photoluminescence in Undoped GaN Films. *Phys. Rev. B* **2001**, *64*, 115205.
59. Hugues, M.; Damilano, B.; Duboz, J.-Y.; Massies, J. Exciton Dissociation and Hole Escape in the Thermal Photoluminescence Quenching of (Ga, In)(N,As) Quantum Wells. *Phys. Rev. B* **2007**, *75*, 115337.
60. Ishii, R.; Funato, M.; Kawakami, Y. Huge Electron-Hole Exchange Interaction in Aluminum Nitride. *Phys. Rev. B* **2013**, *87*, 161204(R).
61. Krustok, J.; Collan, H.; Hjelt, K. Does the Low-Temperature Arrhenius Plot of the Photoluminescence Intensity in CdTe Point Towards an Erroneous Activation Energy? *J. Appl. Phys.* **1997**, *81*, 1442–1445.
62. Shi, H. L.; Pan, H.; Zhang, Y. W.; Yakobson, B. I. Quasiparticle Band Structures and Optical Properties of Strained Monolayer MoS_2 and WS_2. *Phys. Rev. B* **2013**, *87*, 155304.
63. Berkelbach, T. C.; Hybertsen, M. S.; Reichman, D. R. Theory of Neutral and Charged Excitons in Monolayer Transition Metal Dichalcogenides. *Phys. Rev. B* **2013**, *88*, 045318.
64. Ramasubramaniam, A. Large Excitonic Effects in Monolayers of Molybdenum and Tungsten Dichalcogenides. *Phys. Rev. B* **2012**, *86*, 115409.
65. Cheiwchanchamnangij, T.; Lambrecht, W. R. L. Quasiparticle Band Structure Calculation of Monolayer, Bilayer, and Bulk MoS_2. *Phys. Rev. B* **2012**, *85*, 205302.
66. Komsa, H. P.; Krasheninnikov, A. V. Effects of Confinement and Environment on the Electronic Structure and Exciton Binding Energy of MoS_2 from First Principles. *Phys. Rev. B* **2012**, *86*, 241201(R).
67. Sallen, G.; Bouet, L.; Marie, X.; Wang, G.; Zhu, C. R.; Han, W. P.; Lu, Y.; Tan, P. H.; Amand, T.; Liu, B. L.; Urbaszek, B. Robust Optical Emission Polarization in MoS_2 Monolayers through Selective Valley Excitation. *Phys. Rev. B* **2012**, *86*, 081301(R).
68. Varshni, Y. P. Temperature Dependence of Energy Gap in Semiconductors. *Physica* **1967**, *34*, 149–154.
69. Odonnell, K. P.; Chen, X. Temperature-Dependence of Semiconductor Band-Gaps. *Appl. Phys. Lett.* **1991**, *58*, 2924–2926.
70. Frantsuzov, P.; Kuno, M.; Janko, B.; Marcus, R. A. Universal Emission Intermittency in Quantum Dots, Nanorods and Nanowires. *Nat. Phys.* **2008**, *4*, 519–522.
71. Frantsuzov, P. A.; Volkan-Kacso, S.; Janko, B. Universality of the Fluorescence Intermittency in Nanoscale Systems: Experiment and Theory. *Nano Lett.* **2013**, *13*, 402–408.
72. Htoon, H.; O'Connell, M. J.; Cox, P. J.; Doorn, S. K.; Klimov, V. I. Low Temperature Emission Spectra of Individual Single-Walled Carbon Nanotubes: Multiplicity of Subspecies within Single-Species Nanotube Ensembles. *Phys. Rev. Lett.* **2004**, *93*, 027401.